Volume 21
Number 6
14 February 2025
Pages 1029–1242

Soft Matter

rsc.li/soft-matter-journal

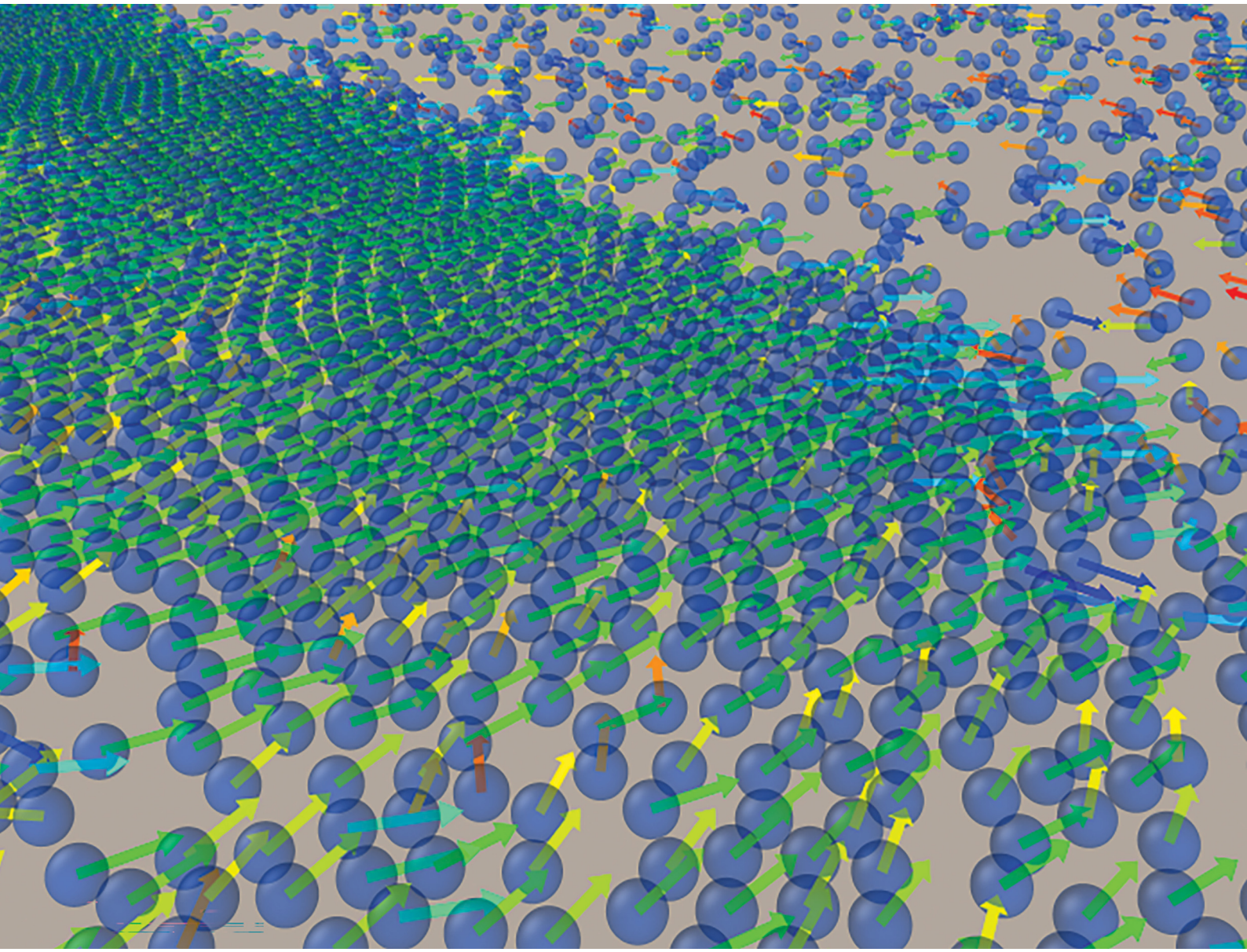

ISSN 1744-6848

ROYAL SOCIETY OF CHEMISTRY

PAPER
Juan Pablo Miranda, Demian Levis and Chantal Valeriani
Collective motion of energy depot active disks

20 YEARS ANNIVERSARY

Soft Matter

PAPER

View Article Online
View Journal | View Issue

Check for updates

Cite this: *Soft Matter*, 2025, **21**, 1045

Collective motion of energy depot active disks†

Juan Pablo Miranda, *[ab] Demian Levis *[cd] and Chantal Valeriani [ab]

Received 26th June 2024,
Accepted 18th November 2024

DOI: 10.1039/d4sm00785a

rsc.li/soft-matter-journal

In the present work we have studied collectives of active disks with an energy depot, moving in the two-dimensional plane and interacting *via* an excluded volume. The energy depot accounts for the extraction of energy taking place at the level of each particle in order to perform self-propulsion, included in an underdamped Langevin dynamics. We show that this model undergoes a flocking transition, exhibiting some of the key features of the Vicsek model, namely, band formation and giant number fluctuations. These bands, either single or multiple, are dense and very strongly polarised propagating structures. Large density bands disappear as the activity is further increased, eventually reaching a homogeneous polar state. We unravel an effective alignment interaction at the level of two-particle collisions that can be controlled by activity and gives rise to flocking at large scales.

Open Access Article. Published on 18 November 2024. Downloaded on 1/20/2026 9:26:51 PM.
This article is licensed under a Creative Commons Attribution-NonCommercial 3.0 Unported Licence.

1 Introduction

Active matter systems, composed of a collection of interacting self-propelled units, have been the focus of a great deal of research efforts over the last decades.[1–3] Given that they are not in equilibrium, these systems exhibit a number of large-scale phenomena, not detected in equilibrium systems. A salient example is the emergence of collective motion, widely observed both in the living world and in synthetic realizations of active particles designed in the laboratory.[4,5] Collective motion has been reported in a broad range of time and length scales, ranging from systems made of 10^{-7}–10^{-6} m objects (*e.g.* actomyosin networks,[6] bacteria[7–9] and colloidal suspensions[10,11]) up to systems composed of agents of the order of $\sim$1 m in size (*e.g.* animal groups[12]).

To gain a theoretical insight into this seemingly common feature displayed by a large variety of active systems of self-propelled units, simple models have been proposed, such as active Brownian particles,[13] the Vicsek model[14] together with their continuum hydrodynamic descriptions.[14–17] Spherical active Brownian particles have been shown to exhibit phase separation even when interacting only repulsively. This phase separation is induced by self-propulsion and appears in dense enough situations.[17] Whereas the Vicsek model describes the behaviour of self-propelled aligning particles, propelled at a constant speed and solely interacting *via* velocity-alignment interactions, being ferromagnetic/polar or nematic.[5] In two dimensions, a collection of polarly aligning self-propelled particles exhibits a flocking transition towards a collectively moving state, the emergence of which is typically accompanied by large density heterogeneities in the form of traveling bands.[18,19] Beyond the ideal case in which particles are just point-like, aligning particles have also been demonstrated to undergo a flocking transition, with the emergence of band-like patterns, even when repulsive interactions are taken into account.[20–23] These works suggest that neither excluded-volume interactions nor collision rules are enough to change the phenomenology of the order–disorder transition in the Vicsek model. Flocking can also arise from particles' shape (*e.g.* self-propelled rod-like particles aligning upon collision[24,25]) or from collisions between spherical particles which are not momentum conserving, such as vibrated polar grains[26–28] (the latter are typically modeled as particles 'self' re-orienting their direction of self-propulsion with the one of their instantaneous velocity[29–32]).

Although self-propulsion needs an energy intake from the environment (or from an internal fuel) to convert it into motion in the presence of dissipation, Vicsek-type models and other simple active particle descriptions do not consider it explicitly. These models describe a system of active particles at a larger mesoscopic scale, somehow coarse-graining the microscopic details of the self-propulsion mechanism. One of the earliest models of active particles[33] explicitly considering an internal energy intake leading to self-propulsion is the so-called energy depot model.[34] The dynamics of such an energy depot active particle (EDAP) model has been thoroughly studied in the past, mostly considering medium-mediated inter-particle interactions[35]

[a] *Departamento de Estructura de la Materia, Física Térmica y Electrónica, Universidad Complutense de Madrid, Madrid 28040, Spain. E-mail: juanpami@ucm.es*
[b] *GISC - Grupo Interdisciplinar de Sistemas Complejos, Madrid 28040, Spain*
[c] *Computing and Understanding Collective Action (CUCA) Lab, Condensed Matter Physics Department, Universitat de Barcelona, Marti i Franquès 1, Barcelona 08028, Spain. E-mail: levis@ub.edu*
[d] *University of Barcelona Institute of Complex Systems (UBICS), Martí i Franquès 1, Barcelona E08028, Spain*

† Electronic supplementary information (ESI) available. See DOI: https://doi.org/10.1039/d4sm00785a

Open Access Article. Published on 18 November 2024. Downloaded on 1/20/2026 9:26:51 PM.
This article is licensed under a Creative Commons Attribution-NonCommercial 3.0 Unported Licence.

or their dynamics in an external potential.[36–38] This model has proven useful for a stochastic thermodynamic description of active matter,[39,40] even though most authors have used active Brownian particles[41,42] and active Ornstein–Uhlenbeck particles[43,44] for this purpose.

As far as we know, the collective behavior of dense suspensions of EDAP with excluded volume interactions has not been explored so far. Other works have focused on modifying the model considering different assumptions, leading to substantial differences in diffusivity and transport properties, such as the effect of cross-correlated noise,[45,46] a braking mechanism,[47,48] the coupling of a load to an energy depot particle[49] and even their motion in disordered media where their propulsion is coupled to the properties of the latter.[50]

In the present work, we consider repulsive spherical EDAP (disks) in two dimensions. We show that the mere competition between crowding effects and self-propulsion is enough to trigger a flocking transition, exhibiting some of the key features of Vicsek model's phenomenology, namely band formation and giant number fluctuations. As compared to suspensions of active Brownian particles, where motility-induced phase separation is observed,[17] our system of repulsive spherical EDAP does not show evidence of such a phenomenon. Moreover, ABP suspensions undergo fluid–hexatic and hexatic–solid transitions at higher densities.[51] Here we focus instead on the emergence of collective motion in a system of repulsive, non-polar, spherical EDAP, putting aside the investigation of the phase transitions associated with 2d melting at larger densities.

In the 'density-activity' plane plotted in Fig. 1, we report the value of the global polar order parameter for different state points, using a color code ranging from yellow (high polarity) to blue (low polarity). Each state point (represented by a circle) corresponds to an independent numerical simulation of a system with $N = 2000$ disks. Beyond a given threshold in density and/or activity, the system sets in a collectively moving state. The transition towards such a state is accompanied by the formation of large density bands that disappear as the activity is further increased, eventually reaching a homogeneous polar state. To understand this behaviour, we extract an effective interaction *via* the radial distribution function and find that pair-collisions lead to an effective alignment that can be controlled by activity and is responsible for the flocking transition to occur.

The paper is structured as follows: in Section 2 we define the model and its different regimes; in Section 3 we focus on the identification and characterisation of collective motion; in Section 4 we shed light on the origins of the reported flocking behaviour in the absence of explicit alignment, showing that an effective alignment interaction emerges from two-particle collisions.

2 Model for self-propelled particles with an energy depot

We consider a two dimensional suspension of N particles whose position and velocities are $\mathbf{r}_i$ and $\mathbf{v}_i$, respectively. Each particle

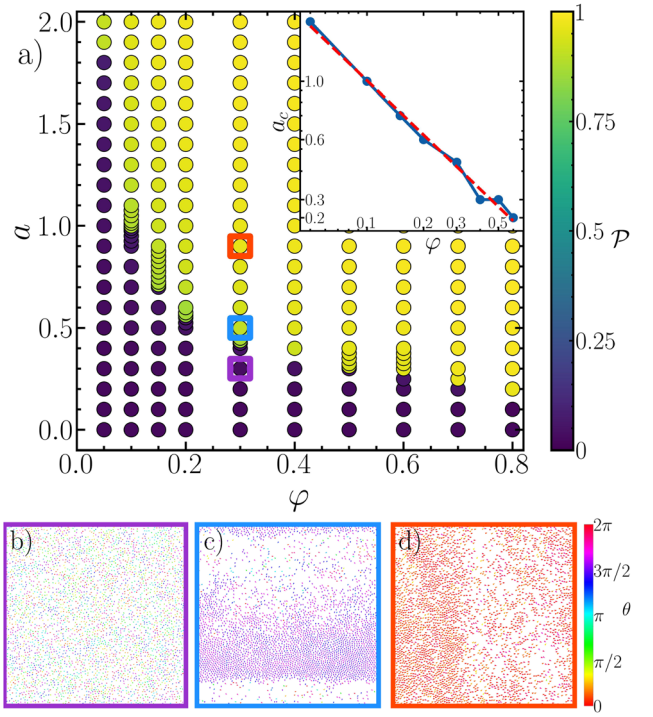

Fig. 1 (a) State diagram for a system of $N = 2000$ particles representing the values of activity and area fraction according to which the system is in a disordered or polar state, as indicated by a color map of the steady state global polarisation. The inset shows the activity threshold $a_c(\varphi)$ (in log–log scale) above which we observe collective motion (extracted as the maximum of the susceptibility). The dashed red line corresponds to a power-law decay $\sim\varphi^{\lambda}$, with $\lambda = -0.77$. The colored squares indicate the location of the snapshots shown below in the ($\varphi - a$) plane. Snapshots of the steady state of $N = 10\,000$ systems at $\varphi = 0.3$: (b) $a = 0.3$, homogeneous and disordered states; (c) $a = 0.5$, dense polar band surrounded by a (dilute) disordered background; (d) $a = 0.9$, a polar state with a more homogeneous density distribution.

carries an internal energy depot ε_i, describing the conversion of energy extracted from the environment into kinetic energy at the level of individual particles. The dynamics of ε_i is over-damped and given by[33,34]

$$\dot{\varepsilon}_i(t) = q - c\varepsilon_i(t) - d\mathbf{v}_i^2\varepsilon_i(t) \quad (1)$$

The parameters q, c and d quantify the rate of energy intake, energy dissipated and conversion into kinetic energy, respectively. The motion of each particle is then governed by the following Langevin equation:

$$m\dot{\mathbf{v}}_i = -(\gamma_0 - d\varepsilon_i(t))\mathbf{v}_i - \sum_{j\neq i}\nabla U(r_{ij}) + \sqrt{2D}\xi_i(t) \quad (2)$$

where $U(r_{ij})$ is the inter-particle repulsive interaction and ξ is a Gaussian white noise of zero mean and unit variance, mimicking a thermal bath at temperature T. The damping coefficient γ_0 (obeying $D = \gamma_0 k_B T$) is combined with the internal energy depot term. The energy depot acts on each particle as a self-propulsion force: indeed, it appears as an advective term, which can be cast as an effective velocity-dependent damping coefficient $\gamma(\mathbf{v}_i) = \gamma_0 - d\varepsilon_i(t)$. If $\gamma(\mathbf{v}) < 0$ the particle is accelerated by the effect of the energy depot, while in the opposite case it is

This journal is © The Royal Society of Chemistry 2025

Open Access Article. Published on 18 November 2024. Downloaded on 1/20/2026 9:26:51 PM.
This article is licensed under a Creative Commons Attribution-NonCommercial 3.0 Unported Licence.

still damped but with a smaller damping coefficient than γ_0. In the adiabatic limit, considering that the energy depot is the fastest degree of freedom, the equations of motion are simplified to

$$m\dot{\mathbf{v}}_i = -\gamma(\mathbf{v}_i)\mathbf{v}_i - \sum_{j\neq i}\nabla U(r_{ij}) + \sqrt{2D}\xi_i(t). \quad (3)$$

with

$$\gamma(\mathbf{v}) = \gamma_0\left(1 - \frac{a}{b+\mathbf{v}^2}\right) \quad (4)$$

where we have introduced, to reduce the number of parameters, $a = q/\gamma_0$ and $b = c/d$. EDAP exhibits different dynamic regimes depending on the values of these parameters.[34] Eqn (4) is obtained by setting $\dot{\varepsilon}_i(t) = 0$ in eqn (1) and then injecting its solution in Eqn (2). In Fig. 2(b) we represent the different dynamic regimes in terms of the behaviour of $\gamma(\mathbf{v})$. We denote $\mathbf{v}_0 = \sqrt{a-b}$, the velocity for which $\gamma(\mathbf{v}_0) = 0$, being $a > b$ (orange line). We can then identify two different situations depending on the value of the velocity with respect to this reference. For $\mathbf{v} > \mathbf{v}_0$ the motion is damped with $0 < \gamma(\mathbf{v}) < \gamma_0$, approaching the passive limit as $\mathbf{v}$ increases. Meanwhile, for $\mathbf{v} < \mathbf{v}_0$, $\gamma(\mathbf{v}) < 0$, meaning that the energy depot accelerates the motion in the direction of $\mathbf{v}$. Eventually, as the particle accelerates, it reaches a velocity close to $\mathbf{v}_0$, above which its motion is damped. All in all, the average velocity of a single EDAP is $\mathbf{v}_0$.[34] For $a < b$, particles always exhibit damped Brownian motion as $\gamma(\mathbf{v})$ remains positive (blue and green lines in Fig. 2). The passive limit is recovered when $a \to 0$, allowing for a smooth connection with a well-known equilibrium system. We shall thus identify a as our activity parameter, and consider the other energy depot parameters as fixed. For a single particle the mean-square displacement reads, in the weak noise (strong pumping) approximation[34,52]

$$\Delta r^2(t) = \langle(\mathbf{r}(t) - \mathbf{r}(0))^2\rangle \approx 4D^{\text{eff}}\left\{t + \tau\left[\exp\left(-\frac{t}{\tau}\right) - 1\right]\right\}, \quad (5)$$

showing thus persistent random motion with effective diffusivity $D^{\text{eff}} = \mathbf{v}_0{}^4/2k_BT\gamma_0 \propto (a-b)^2$ and persistence time $\tau = \mathbf{v}_0{}^2/2k_BT\gamma_0 \propto a - b$. Thus, varying a allows us to disentangle the role played by activity and move across the different dynamic regimes. In Fig. 2(a) we put eqn (5) into test and run numerical simulations to extract estimates of the parameters $\mathbf{v}_0$, τ and D^{eff} (see Fig. 2 panels (c)–(e)). It is worth mentioning that D^{eff}, $\mathbf{v}_0$ and τ are ill-defined when $a < b$, while they increase with a once the active regime is reached (quadratically and linearly, respectively). Then, in the following, we consider a as the activity control parameter. Eqn (5) is obtained in the strong pumping approximation, namely, from the assumption that the particle velocity has relaxed to $\mathbf{v}_0$ (its relaxation to this value is omitted). Therefore, one expects a good agreement between the simulation data and this analytical result only at long-enough times (longer than the relaxation of the velocity), as shown in Fig. 2(a).

The interactions between particles derive from a pairwise potential $U(r_{ij} = |\mathbf{r}_i - \mathbf{r}_j|)$, that here we choose to be purely repulsive and short-range. In practice, we use the following

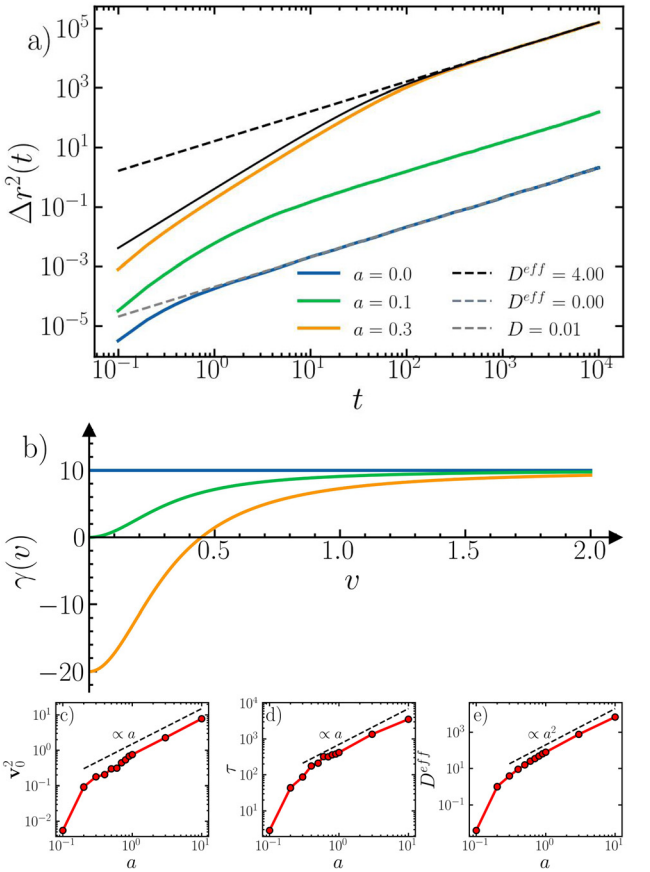

Fig. 2 (a) MSD of non-interacting energy depot particles for different degrees of activity at fixed $\gamma_0 = 10$, $k_BT = 5.10^{-4}$ and $b = 1/10$. The black solid line represents the analytical expression (5) for a system with $a = 0.3$. Discontinuous lines represent the long time diffusive behavior with the effective diffusivity given in the key. The blue line represents a system with $a = 0$, *i.e.*, in the Brownian case. The green line corresponds to the limit case $a = b$. The orange line represents a system in the regime $a > b$ with $a = 3$. (b) Different values of $\gamma(\mathbf{v})$ depending on their velocity for the corresponding colors of panel a. We extract, by fitting our data to eqn (5), $\mathbf{v}_0{}^2$ (panel c), τ (panel d) and D^{eff} (panel e), and compare them to the expected scaling with a.

WCA form:[53]

$$U(\mathbf{r}_{ij}) = \begin{cases} 4u_0\left[\left(\frac{\sigma}{r_{ij}}\right)^{12} - \left(\frac{\sigma}{r_{ij}}\right)^{6} + \frac{1}{4}\right], & r_{ij} \leqslant 2^{1/6}\sigma \\ 0, & r_{ij} \geqslant 2^{1/6}\sigma \end{cases} \quad (6)$$

where σ is the particle's diameter.

We simulate a system of N active particles in an $L \times L$ box with periodic boundary conditions and area fraction $\varphi = \frac{N\pi\sigma^2}{4L^2}$. The Langevin dynamics has been implemented by means of the LAMMPS[54] open source package, making use of the Velocity Verlet integrator. In order to perform these simulations we have used different initial configurations. At intermediate densities, we have started from random positions and velocities (uniformly distributed); whereas at higher densities we have

Open Access Article. Published on 18 November 2024. Downloaded on 1/20/2026 9:26:51 PM.
This article is licensed under a Creative Commons Attribution-NonCommercial 3.0 Unported Licence.

located particles in an ordered square lattice, with again random velocities.

All physical quantities are expressed in Lennard–Jones reduced units, with lengths, times and energies given in terms of $\sigma = \tau_{LJ} = u_0 = 1$, where $\tau_{LJ} = \sqrt{m\sigma^2/u_0}$ and $m = 1$. We have run simulations of systems with $N = 2000$ up to 30 000 particles at different area fractions φ, in the range $\varphi = 0.05, \ldots, 0.8$. In our simulations, we set $\gamma_0 = 10$, the time step to $\Delta t/\tau_{LJ} = 10^{-3}$ and the reduced temperature $k_B T/u_0 = 5 \times 10^{-4}$. We explore the collective behavior of the model at fixed $b = 1/10$ as a function of both a and φ. In practice, due to the extent of the parameter space in the model, we choose to fix c, d and γ_0, while the activity a is varied changing the values of q. As we group the parameters, this choice is equivalent to varying the parameter a while fixing b. The values of the original parameters were $c = 1$, $d = 10$ and q varying between 0 and 30. This is equivalent to vary a from 0 to 3. The chosen parameters allow us to set an energy scale (being c directly proportional to the depot internal energy) and to explore different dynamical regimes by only varying a (having chosen a small value for b). It has to be taken into account the fact that systems with $a < b$ cannot be considered motile, even though we have also studied them.

3 Transition to a flocking state

To quantify collective motion, we employ the global polar order parameter $\mathscr{P}$, or polarisation, given by the modulus of the average direction of the instantaneous velocity vector of each particle

$$P = \left\langle \left| \frac{1}{N} \sum_{i=1}^{N} \mathbf{e}_i \right| \right\rangle, \tag{7}$$

where $\mathbf{e}_i$ is the orientation of the velocity vector of particle i, given by $\mathbf{e}_i = \mathbf{v}_i/|\mathbf{v}_i| = (\cos\theta_i, \sin\theta_i)$, and $\langle\cdot\rangle$ denotes a steady-state average. Values of $\mathscr{P} > 0$ indicate that a fraction of the particles is aligned, thus moving coherently, whereas $\mathscr{P} = 0$ corresponds to particles moving in random directions.

Fig. 3(a) represents the values of polarisation obtained for a range of activities and area fractions φ (as indicated in the legend). Increasing activity, at a fixed φ, we observe a disorder (low polar order) to order (high polar order) transition. Interestingly, the value of a beyond which the transition takes place depends on the system area fraction, decreasing when the area fraction increases. To establish the robustness of this transition and the relevance of finite-size effects, we have performed simulations at the same $\varphi = 0.3$ and for different system sizes. As shown in Fig. 3(b), the disorder-to-order transition is always present and the value of activity needed for the transition to take place is not significantly affected by the system size (in the chosen parameter range).

Polar order appears in a suspension of EDAP repulsive particles, in the absence of a prescribed orientation and an explicit alignment rule akin to Vicsek-like models.[14] Particle activity (as a self-propulsion) is controlled by a velocity dependent friction $\gamma(\mathbf{v})$, which changes its modulus in the under-damped

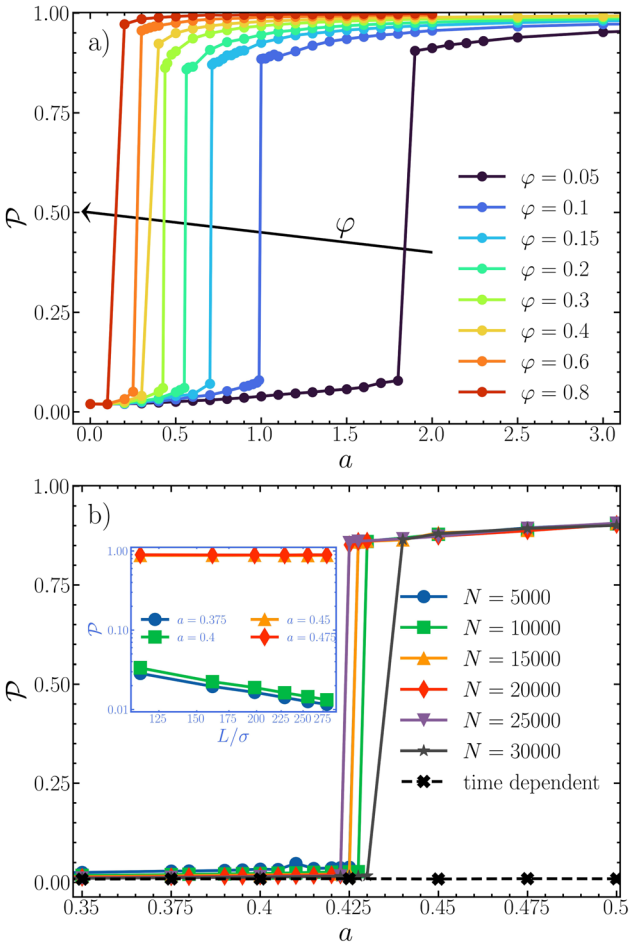

Fig. 3 (a) Polar order parameters as a function of a for different φ in a system of $N = 2000$ particles. The different colors represent different area fractions φ (the arrow indicates increasing values of φ). (b) Polarisation as a function of a at fixed $\varphi = 0.3$ for systems with $N = 5000, \ldots, 30\,000$ particles, and corresponding system sizes $L/\sigma = 114.41, \ldots, 280.25$. The inset of the figure represents the polar order for different linear sizes below and above the onset of flocking. The black line (crosses) corresponds to the time dependent energy depot.

regime. Thus when a particle's self propulsion strength overcomes the particle's rotational noise, the persistence length of the particle increases resulting in a local alignment of colliding particles. The emergence of flocking, typical of polar systems, is caused by particle interactions controlled by activity when self propulsion overcomes rotational noise. More examples of particles with polar order without an explicit alignment have been earlier reported.[10,26,55] In ref. 26 the authors describe experiments on a two dimensional system of disks with a "built-in polar asymmetry" (due to an asymmetric mass distribution). These studies and more recent ones underlined the existence of particles' alignment through collisional arguments using kinetic theory.[56,57] Unlike these works, our system is made of isotropically interacting particles whose activity is encoded in a velocity-dependent friction, resulting in the velocity to change its modulus in an under-damped regime. To explain the observed flocking, we quantify two-body effective interactions,[23,58,59] showing how it develops a tendency to align particle's velocity as activity is

This journal is © The Royal Society of Chemistry 2025

Open Access Article. Published on 18 November 2024. Downloaded on 1/20/2026 9:26:51 PM.
This article is licensed under a Creative Commons Attribution-NonCommercial 3.0 Unported Licence.

increased. A heuristic argument based on particle collisions is presented in Section 4.

Briefly, we have found that collisions favour alignment *via* the combined effect of self-propulsion in the direction of the particles' velocities and steric repulsion. When two particles collide, repulsive forces accelerate them longitudinally. Their speed is thus reduced and activity thus pushes them along a direction that will typically reduce the angle between their velocities. As the rate of collisions increases with density, the onset of flocking decays with φ.

Fig. 1(a) shows the region in parameter space where flocking occurs (in yellow). To detect the onset of collective motion we measure the parameter a_c. First, we calculate the susceptibility as the variance of the order parameter: $\Delta\mathscr{P} = \langle\mathscr{P}^2\rangle - \langle\mathscr{P}\rangle^2$, and denote a_c the activity corresponding to the maximum of the susceptibility. The inset represents the activity threshold $a_c(\varphi)$ above which we detect collective motion: a_c decays with the area fraction (in a way that phenomenologically suggests $a_c \sim \varphi^{-0.77}$).

As shown in Fig. 1(b)–(d) the system in steady state displays different structures. To better understand the nature of the transition towards collective motion, we characterize the structural properties of the different states by computing the probability density of the local order parameter $F(\mathscr{P}_l)$ and the local area fraction $G(\varphi_i)$. The local polar order parameter $\mathscr{P}_l$ is obtained from dividing the system into 100 square cells and computing the average polarisation of the particles inside each one. The local area fraction $G(\varphi_i)$ is obtained from a Voronoi tessellation. Based on the results of local density and polarisation, presented in Fig. 4, we identify three states, reported in Fig. 1(b)–(d). The first one (Fig. 1(b)) is the disordered state, which corresponds to a homogeneous density distribution centered around the mean density (orange and green curves in Fig. 4(a)), and a homogeneous local polarisation distribution (orange and green curves in Fig. 2(b)) corresponding to the absence of polar ordering. With increasing activity we detect a transition to an ordered phase. Beyond the onset of flocking one can identify two different states based on their local density and polarisation. A heterogeneous state (Fig. 1(c)) is observed close to the transition, for which $G(\varphi_i)$ is no longer uni-modal, but displays two maximum values (one at low and one at high densities), indicating a dense region coexisting with a dilute disordered background (see $a = 0.45$, Fig. 4(a)). Interestingly, heterogeneity in the distribution of polarisation coincides with this density heterogeneity. As shown in Fig. 4(b), $F(P)$ exhibits a sharp peak close to 1 with a very broad tail at smaller values, signaling large fluctuations. Such states, as illustrated in Fig. 1(c) correspond to traveling bands, as typically observed in models of flocking. Bands are dense and very strongly polarized propagating structures. A dynamical state of single and multiple band structures is observed at very long times, see ref. 60. The band profile is again reminiscent to the one found in the Vicsek system.[19] As expected, particles in the band accumulate at the front and are better oriented than particles located at the dilute part of the band.

Increasing activity even further, density heterogeneities disappear, and $G(\varphi_i)$ presents a uniform distribution again, although broader than in the small activity limit (see Fig. 4(a)). This regime corresponds to the emergence of a homogeneous polar state (Fig. 1(d)). The polarisation distribution now exhibits a sharp peak close to 1, whose width decreases with increasing activity. So far, we have only detected band formation for intermediate densities close to the transition, quickly disappearing upon increasing activity.

As known from the literature of polar fluids,[61] giant number fluctuations typically appear in the flocking phase. We measure the number density fluctuations to unravel possible connections between orientational order and giant number fluctuations. To do so, we divide the system into 2^k cells and count the number of particles in each cell, considering a large number of configurations, to estimate the mean number of particles $\langle N\rangle$ and its variance ΔN. We repeat the procedure over boxes with different sizes (ranging from $k = 2, \ldots, 8$) and obtain a value of $\langle N\rangle$ for each box size. We then extract a power-law relation $\Delta N \sim N^{\alpha}$ where a value $\alpha > 1/2$ signals giant number fluctuations.

Fig. 5 shows the variance of the number of particles ΔN as a function of the mean number of particles for systems at fixed density ($\phi = 0.3$) but varying the value of the activity parameter. In all cases, $\Delta N \sim N^{\alpha}$. However, as clearly shown in the inset, depending on the activity, the exponent α noticeably varies, jumping from values around 1/2 to almost 1 when $a \approx a_c$. When $\alpha > 0.5$ the system exhibits giant number fluctuations. As shown in Fig. 5, this occurs beyond the onset of flocking. When $\alpha \approx 0.5$, number fluctuations follow what one expects from the central limit theorem. The variation on the value of α with the activity parameter thus provides a complementary way of locating the onset of flocking. When the system sets into the homogeneously dense polar state, at large values of a, we find a

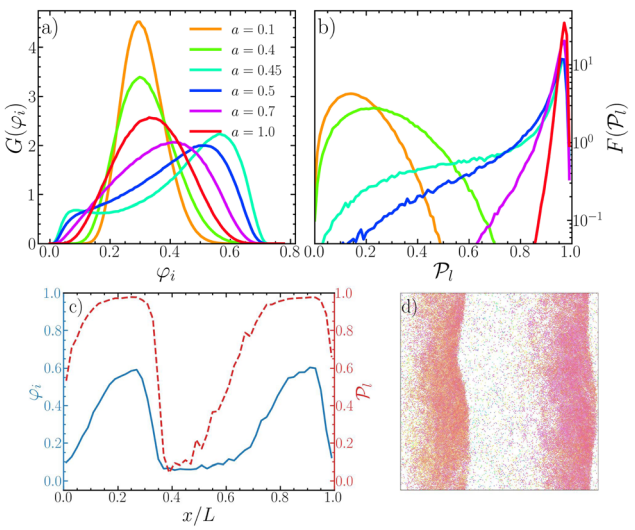

Fig. 4 (a) Local area fraction probability distribution $G(\varphi_i)$ calculated *via* Voronoi tessellations for systems of $N = 10\,000$, $\varphi = 0.3$ and different values of $a = 0.1, \ldots, 1$. (b) Probability distribution function of the order parameter $F(\mathscr{P})$ (same parameters as panel a). (c) Local area fraction φ_i (in blue) and local polar order $\mathscr{P}_l$ profiles along the x direction, across two bands, in a system with $N = 30\,000$, $\varphi = 0.3$ and $a = 0.45$. (d) Snapshot of the system corresponding to the profiles shown in (c).

Open Access Article. Published on 18 November 2024. Downloaded on 1/20/2026 9:26:51 PM.
This article is licensed under a Creative Commons Attribution-NonCommercial 3.0 Unported Licence.

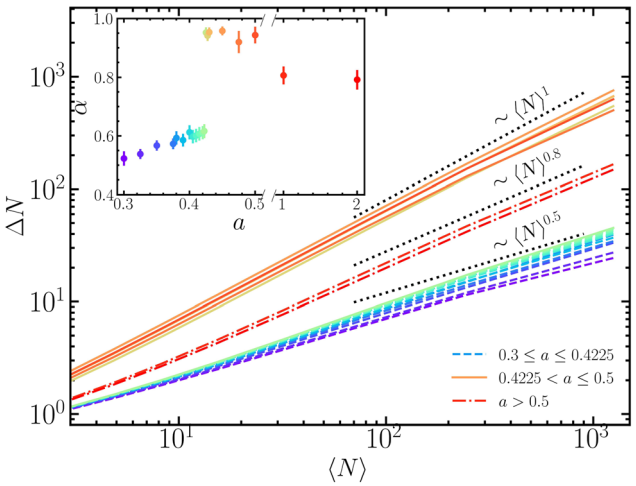

Fig. 5 Variance of the number of particles ΔN compared to its mean $\langle N \rangle$ for systems of N = 20 000 particles, φ = 0.3 and different values of a ranging from 0.3 to 2. Curves (and points in the inset) are colored according to their degree of activity. Dashed lines correspond to a values below the transition, solid lines above, in the band regime, dashed–dotted lines represent two systems in the homogeneous polar fluid regime. The inset shows the dependency of the α exponent with a as extracted from the data in the main panel.

value $\alpha \approx 0.8$, still exhibiting large number fluctuations, although with a smaller exponent than the one in the band regime. This value of $\alpha \approx 0.8$ is close to the value of 0.725 reported by Deseigne *et al.*[26] for vibrated polar disks, and coincides with the exponent of 0.8 in the Vicsek system reported by Chaté *et al.*[19]

4 Understanding the effective alignment

Even though many body interactions might be relevant to understand collective phenomena in active particle systems,[62] one might start with unraveling the emergence of collective motion from the analysis of two body interactions.

To understand whether the emergent behavior is due to pair interactions, we compute the two-particle pair correlation function, depending on both the inter-particle distances and the relative orientation of their velocities. This function can be defined as (ref. 63 and 64)

$$g(r,\theta) = \frac{A}{N^2}\left\langle \sum_i \sum_{j\neq i} \frac{\delta(r - r_{ij})}{r}\delta(\theta - \theta_{ij}) \right\rangle \qquad (8)$$

where $r_{ij} = |\mathbf{r}_i - \mathbf{r}_j|$ is the distance between two disk centres and $\theta_{ij} = \theta_i - \theta_j$ is the relative angle formed by their velocities. We numerically computed $g(r,\theta)$ from two particle simulations. The results are shown in Fig. 6. While in the passive system (left-hand side) $g(r,\theta)$ is isotropic, in the presence of activity (right-hand side) it shows a strong anisotropy, with a pronounced peak for values close to $\theta = 0$, fading to zero as the relative angle moves away. This means that particles' velocities are more likely to point along the same direction. Such correlation is

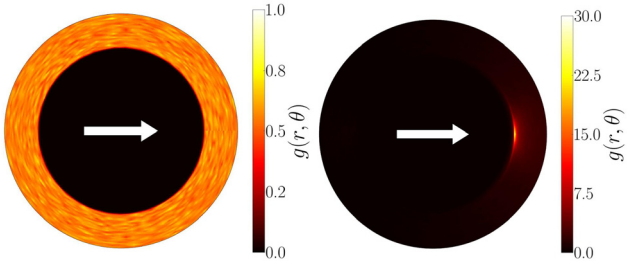

Fig. 6 Pair distribution $g(r,\theta)$ function for a = 0 (left) and a = 1 (right). The angles represent relative orientation between velocities and the color plots the numerical values. The thick arrow indicates the perfectly aligned direction.

localized at contact and quickly decays for r larger than the particle's radius. This shows that the competition between self-propulsion and steric effects gives rise to an effective alignment.

To further quantify such alignment, we extract an effective potential from the radial distribution and study its behavior in terms of the different parameters (such as the activity). This procedure has been conducted earlier to estimate effective interactions between Active Brownian Particles.[23,58,59] Assuming that $g(r,\theta) = \exp(-\beta U_{\text{eff}}(r,\theta))$, one can map the radial distribution function to an effective potential. Fig. 7 shows the effective potential as a function of the angle (panel a) and the effective potential as a function of the inter-particle distance, for varying values of the activity parameter a (panel b). On the one hand, as reported in Fig. 7(a), activity lowers the minima of the potential, favoring an effective alignment: U_{eff} is lowered as a increases for relative angles close to 0, thus increasing the effective alignment as self propulsion is increased. On the other hand, as shown in Fig. 7(b), the minimum of the effective potential corresponds to the cutoff of the WCA potential $r = 2^{1/6}\sigma \simeq 1.12\sigma$. This reveals that the alignment arises from the interplay between the excluded volume interactions and activity.

Since the only interactions are given through excluded volume, the mechanism for alignment has to be mediated by contact interactions (collisions), explaining why the minima of the effective potential occurs at the contact distance between two particles. This also has to do with the fact that the other part of the mechanism is the active force, as the effective potential develops a deeper minimum as activity is increased.

In our model, self-propulsion is controlled by a velocity dependent friction. Particles velocity changes in modulus and direction when particles interact. When two particles collide, their velocity is reduced along the longitudinal, center-to-center direction, while the transverse component remains roughly unchanged at short time scales. Large enough persistence thus generates long collision times, where the longitudinal component of the velocity drops, resulting in a velocity with a larger transversal component, as illustrated in Fig. 8. In this way velocity alignment is induced at the two particle level and this effect is amplified when considering the entire system, thus leading to a polar order at large length scales. Large activity thus induces a velocity alignment in this model, where, as

 This journal is © The Royal Society of Chemistry 2025

Open Access Article. Published on 18 November 2024. Downloaded on 1/20/2026 9:26:51 PM.
This article is licensed under a Creative Commons Attribution-NonCommercial 3.0 Unported Licence.

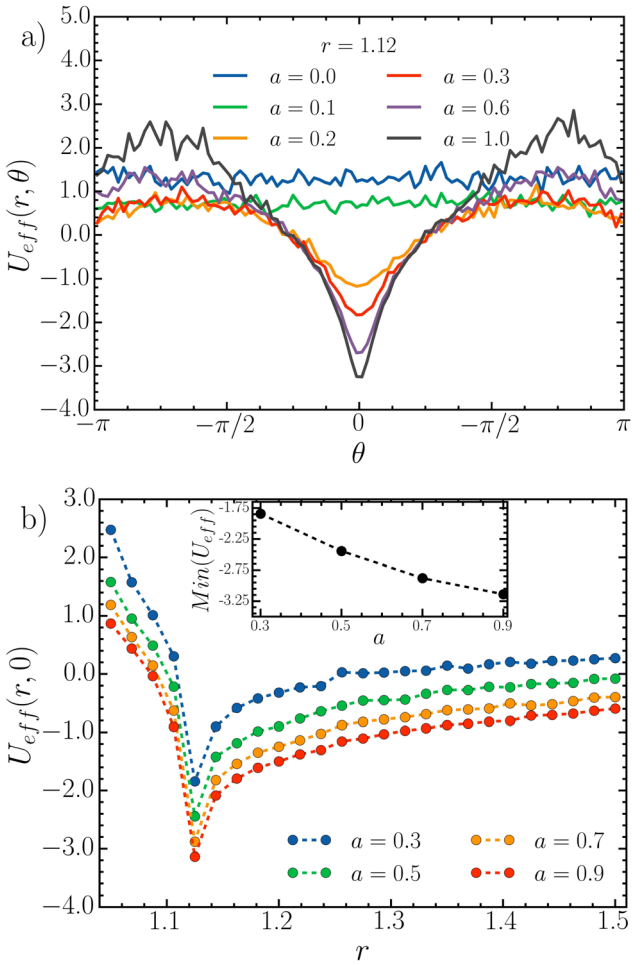

Fig. 7 (a) Effective potential as a function of the relative orientation between particle's velocities at a given inter-particle distance $r = 1.12\sigma$ and different values of a. (b) Effective two particle potential as a function of distance for $\theta = 0$ and different values of a. The inset in the figure shows how the minimum of the potential becomes more pronounced with activity.

compared to active Brownian particles, rotational noise is absent. We show in Fig. 8 a sequence of snapshots during a collision event. The top-right particle hits the other one from behind and it is slowed down by the interaction potential. This makes the collision lasting longer than if the two particles were passive, since the active force is pushing the particle to collide again.

So far, the model defined by eqn (1) and (2) was only considered in the limit in which the internal energy depot relaxes much faster than any other degrees of freedom in the system, *i.e.* the depot is fully over damped. When this assumption is relaxed, we talk about the time dependent energy deport model. We implement the full dynamics of the internal depot by integrating eqn (1) with an Euler scheme. To compare the time dependent model with its adiabatic limit, we have performed a set of simulations for $N = 10\,000$ particles, $\varphi = 0.3$ and a ranging from 0.3 to 2. In this parameter regime, the overdamped model exhibits the characteristic states described above, namely, a is the disordered state, followed by a polar state featuring dense bands and moderate valued of $a > a_c$. Once the full evolution of the energy depot is considered, polar order is lost in this parameter regime, as Fig. 3 shows. The time scale of the energy relaxation, $1/c = 1$, is typically smaller than the persistence time, τ in the regime where flocking is observed. However, in the time-dependent case, the $\dot{\varepsilon}$ term has a faster relaxation that cannot be ignored. As these results are only validated for $b = 0.1$, further parameter exploration could provide a more accurate description on how the polarisation is lost when this time dependence is introduced. The loss of polar order raises the question of whether there is a way to restore it in a different parameter regime, or, eventually, the emergence of other collective states. We leave such an investigation for future work.

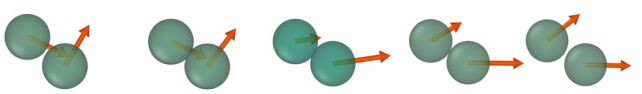

Fig. 8 Successive snapshots during a collision between two particles, where their velocities are represented as orange arrows. The snapshots are ordered from left to right, as time goes on.

5 Conclusions

The present work studied a system of active disks that are self-propelled by an internal energy depot, characterized by a velocity dependent friction and an isotropic repulsive (hard) potential. The novelty of this version of the EDAP model with respect to others is that it presents polar alignment, despite repulsive interactions and not an explicit alignment mechanism. A Vicsek-like transition from a non-polar isotropic state to a polar and ordered state is identified and characterized in terms of the polar order parameter and the giant number fluctuations. The structural analysis reveals the presence of different phases, such as a non-polar homogeneous density phase, and two polar phases. The polar phases are divided into a homogeneously dense and a band phase.

Even though the flocking behavior exhibited by this model resembles the one of the Vicsek model,[19] here the alignment arises from steric collisions in the presence of activity (encapsulated in an internal depot) with no need of an explicit interaction of this kind. Once alignment, controlled by activity, becomes strong enough, flocking occurs, with strong similarities to the well-known phenomenology of Vicsek-type models. As increasing activity increases the tendency of particles to align, the emergence of large-scale polar order is controlled by competition between noise and alignment. Given that the alignment mechanism is not explicit, an explanation is provided in terms of an effective potential originated by collisions between particles. The effective potential reveals a connection between the potential and the activity, which is translated as the torque acting on particles.

From our results, we conclude that this model is a good candidate for more realistic systems of active engines[65] at the micro-scale, since it allows a theoretical approach that could complement numerical simulations (as in ref. 66–68).

Open Access Article. Published on 18 November 2024. Downloaded on 1/20/2026 9:26:51 PM. This article is licensed under a Creative Commons Attribution-NonCommercial 3.0 Unported Licence.

Data availability

The data that support the findings of this study are available from the corresponding author upon reasonable request.

Conflicts of interest

There are no conflicts to declare.

Acknowledgements

C. V. acknowledges funding IHRC22/00002 and PID2022-140407NB-C21 from AEI/MICINN. D. L. acknowledges AEI/MICINN for funding under Project PID2022-140407NB-C22. J. P. M. thanks Miguel Barriuso and José Martín-Roca for helpful scientific discussions.

References

1 M. C. Marchetti, J.-F. Joanny, S. Ramaswamy, T. B. Liverpool, J. Prost, M. Rao and R. A. Simha, *Rev. Mod. Phys.*, 2013, **85**, 1143.
2 M. R. Shaebani, A. Wysocki, R. G. Winkler, G. Gompper and H. Rieger, *Nat. Rev. Phys.*, 2020, **2**, 181–199.
3 C. Bechinger, R. Di Leonardo, H. Löwen, C. Reichhardt, G. Volpe and G. Volpe, *Rev. Mod. Phys.*, 2016, **88**, 045006.
4 T. Vicsek and A. Zafeiris, *Phys. Rep.*, 2012, **517**, 71–140.
5 H. Chaté, *Annu. Rev. Condens. Matter Phys.*, 2020, **11**, 189–212.
6 V. Schaller, C. Weber, C. Semmrich, E. Frey and A. R. Bausch, *Nature*, 2010, **467**, 73–77.
7 F. Peruani, J. Starruß, V. Jakovljevic, L. Søgaard-Andersen, A. Deutsch and M. Bär, *Phys. Rev. Lett.*, 2012, **108**, 098102.
8 A. Sokolov and I. S. Aranson, *Phys. Rev. Lett.*, 2012, **109**, 248109.
9 H. Li, X.-q Shi, M. Huang, X. Chen, M. Xiao, C. Liu, H. Chaté and H. Zhang, *Proc. Natl. Acad. Sci. U. S. A.*, 2019, **116**, 777–785.
10 A. Bricard, J.-B. Caussin, N. Desreumaux, O. Dauchot and D. Bartolo, *Nature*, 2013, **503**, 95–98.
11 A. Kaiser, A. Snezhko and I. S. Aranson, *Sci. Adv.*, 2017, **3**, e1601469.
12 W. Bialek, A. Cavagna, I. Giardina, T. Mora, E. Silvestri, M. Viale and A. M. Walczak, *Proc. Natl. Acad. Sci. U. S. A.*, 2012, **109**, 4786–4791.
13 P. Romanczuk, M. Bär, W. Ebeling, B. Lindner and L. Schimansky-Geier, *Eur. Phys. J.: Spec. Top.*, 2012, **202**, 1–162.
14 T. Vicsek, A. Czirók, E. Ben-Jacob, I. Cohen and O. Shochet, *Phys. Rev. Lett.*, 1995, **75**, 1226–1229.
15 J. Toner and Y. Tu, *Phys. Rev. Lett.*, 1995, **75**, 4326–4329.
16 S. Ramaswamy, *Annu. Rev. Condens. Matter Phys.*, 2010, **1**, 323–345.
17 M. E. Cates and J. Tailleur, *Annu. Rev. Condens. Matter Phys.*, 2015, **6**, 219–244.
18 A. P. Solon, H. Chaté and J. Tailleur, *Phys. Rev. Lett.*, 2015, **114**, 068101.
19 H. Chaté, F. Ginelli, G. Grégoire and F. Raynaud, *Phys. Rev. E: Stat., Nonlinear, Soft Matter Phys.*, 2008, **77**(4 Pt 2), 046113.
20 R. Martinez, F. Alarcon, D. Rogel Rodriguez, J. L. Aragones and C. Valeriani, *Eur. Phys. J. E: Soft Matter Biol. Phys.*, 2018, **41**, 91.
21 J. Barré, R. Chétrite, M. Muratori and F. Peruani, *J. Stat. Phys.*, 2015, **158**, 589–600.
22 E. Sese-Sansa, I. Pagonabarraga and D. Levis, *Europhys. Lett.*, 2018, **124**, 30004.
23 E. Sesé-Sansa, D. Levis and I. Pagonabarraga, *Phys. Rev. E*, 2021, **104**, 054611.
24 M. Bär, R. Großmann, S. Heidenreich and F. Peruani, *Annu. Rev. Condens. Matter Phys.*, 2020, **11**, 441–466.
25 R. Großmann, I. S. Aranson and F. Peruani, *Nat. Commun.*, 2020, **11**, 5365.
26 J. Deseigne, O. Dauchot and H. Chaté, *Phys. Rev. Lett.*, 2010, **105**, 098001.
27 A. Kudrolli, G. Lumay, D. Volfson and L. S. Tsimring, *Phys. Rev. Lett.*, 2008, **100**, 058001.
28 V. Narayan, S. Ramaswamy and N. Menon, *Science*, 2007, **317**, 105–108.
29 B. Szabo, G. Szöllösi, B. Gönci, Z. Jurányi, D. Selmeczi and T. Vicsek, *Phys. Rev. E: Stat., Nonlinear, Soft Matter Phys.*, 2006, **74**, 061908.
30 O. Dauchot and V. Démery, *Phys. Rev. Lett.*, 2019, **122**, 068002.
31 O. Dauchot, *Active Matter and Nonequilibrium Statistical Physics: Lecture Notes of the Les Houches Summer School: Volume 112, September 2018*, 2022, vol. 112, p. 102.
32 M. Paoluzzi, D. Levis and I. Pagonabarraga, *Commun. Phys.*, 2024, **7**, 57.
33 F. Schweitzer, W. Ebeling and B. Tilch, *Phys. Rev. Lett.*, 1998, **80**, 5044–5047.
34 F. Schweitzer and J. D. Farmer, *Brownian agents and active particles: collective dynamics in the natural and social sciences*, Springer, 2003, vol. 1.
35 V. Lobaskin and M. Romenskyy, *Phys. Rev. E: Stat., Nonlinear, Soft Matter Phys.*, 2013, **87**, 052135.
36 F. Schweitzer, W. Ebeling and B. Tilch, *Phys. Rev. E: Stat., Nonlinear, Soft Matter Phys.*, 2001, **64**, 021110.
37 R. Mach and F. Schweitzer, *Bull. Math. Biol.*, 2007, **69**, 539–562.
38 W. Ebeling, F. Schweitzer and B. Tilch, *BioSystems*, 1999, **49**, 17–29.
39 D. Chaudhuri, *Phys. Rev. E: Stat., Nonlinear, Soft Matter Phys.*, 2014, **90**, 022131.
40 U. Seifert, *Annu. Rev. Condens. Matter Phys.*, 2019, **10**, 171–192.
41 G. Szamel, *Phys. Rev. E*, 2019, **100**, 050603.
42 S. Shankar and M. C. Marchetti, *Phys. Rev. E*, 2018, **98**, 020604.
43 É. Fodor, C. Nardini, M. E. Cates, J. Tailleur, P. Visco and F. Van Wijland, *Phys. Rev. Lett.*, 2016, **117**, 038103.
44 L. Caprini, U. M. B. Marconi, A. Puglisi and A. Vulpiani, *J. Stat. Mech.: Theory Exp.*, 2019, **2019**, 053203.
45 Y. Fang, Y. Luo, Z. Ma and C. Zeng, *Phys. A*, 2021, **564**, 125503.

 This journal is © The Royal Society of Chemistry 2025

Open Access Article. Published on 18 November 2024. Downloaded on 1/20/2026 9:26:51 PM.
This article is licensed under a Creative Commons Attribution-NonCommercial 3.0 Unported Licence.

46 L. Guan, Y. Fang, K. Li, C. Zeng and F. Yang, *Phys. A*, 2018, **505**, 716–728.
47 Y. Zhang and C. K. Kim, *et al.*, *New J. Phys.*, 2008, **10**, 103018.
48 Y. Zhang, C. K. Kim, K.-J.-B. Lee and Y. Park, *Eur. Phys. J. E: Soft Matter Biol. Phys.*, 2009, **29**, 345–349.
49 M. Ann and P. J. Park, *et al.*, *Phys. A*, 2015, **436**, 126–134.
50 K. S. Olsen, L. Angheluta and E. G. Flekkøy, *Soft Matter*, 2021, **17**, 2151–2157.
51 P. Digregorio, D. Levis, A. Suma, L. F. Cugliandolo, G. Gonnella and I. Pagonabarraga, *Phys. Rev. Lett.*, 2018, **121**, 098003.
52 A. Mikhailov and D. Meinköhn, *Stochastic Dynamics*, Heidelberg, Berlin, 1997, pp. 334–345.
53 J. D. Weeks, D. Chandler and H. C. Andersen, *J. Chem. Phys.*, 1971, **54**, 5237–5247.
54 A. P. Thompson, H. M. Aktulga, R. Berger, D. S. Bolintineanu, W. M. Brown, P. S. Crozier, P. J. in 't Veld, A. Kohlmeyer, S. G. Moore, T. D. Nguyen, R. Shan, M. J. Stevens, J. Tranchida, C. Trott and S. J. Plimpton, *Comput. Phys. Commun.*, 2022, **271**, 108171.
55 C. A. Weber, T. Hanke, J. Deseigne, S. Léonard, O. Dauchot, E. Frey and H. Chaté, *Phys. Rev. Lett.*, 2013, **110**, 208001.
56 T. Hanke, C. A. Weber and E. Frey, *Phys. Rev. E: Stat., Nonlinear, Soft Matter Phys.*, 2013, **88**, 052309.
57 K.-D. N. T. Lam, M. Schindler and O. Dauchot, *New J. Phys.*, 2015, **17**, 113056.
58 T. F. Farage, P. Krinninger and J. M. Brader, *Phys. Rev. E: Stat., Nonlinear, Soft Matter Phys.*, 2015, **91**, 042310.
59 U. M. B. Marconi, M. Paoluzzi and C. Maggi, *Mol. Phys.*, 2016, **114**, 2400–2410.
60 See ESI†.
61 K.-D. N. T. Lam, M. Schindler and O. Dauchot, *J. Stat. Mech.: Theory Exp.*, 2015, **2015**, P10017.
62 F. Turci and N. B. Wilding, *Phys. Rev. Lett.*, 2021, **126**, 038002.
63 J.-P. Hansen and I. R. McDonald, *Theory of simple liquids: with applications to soft matter*, Academic press, 2013.
64 J. Bialké, H. Löwen and T. Speck, *Europhys. Lett.*, 2013, **103**, 30008.
65 É. Fodor and M. E. Cates, *Europhys. Lett.*, 2021, **134**, 10003.
66 K. Sekimoto, *Stochastic Energetics*, 2010.
67 K. Sekimoto, *Prog. Theor. Phys. Suppl.*, 1998, **130**, 17–27.
68 C. Ganguly and D. Chaudhuri, *Phys. Rev. E: Stat., Nonlinear, Soft Matter Phys.*, 2013, **88**, 032102.